IN-93-CR

14420

P.30

Agency No: NAGW-2023
UAH No: 5-32401
Principal Investigator: John C. Gregory

A MEASUREMENT OF THE ENERGY SPECTRA OF COSMIC RAYS FROM 20 TO 1000 GeV PER AMU

March, 1991
Semi-Annual Report

The University of Alabama in Huntsville

NASA GRANT NO.:	NAGW 2023
TITLE:	A MEASUREMENT OF THE ENERGY SPECTRA OF COSMIC RAYS FROM 20 TO 1000 GeV PER AMU.
REPORTING PERIOD:	1st. Sept. 1990 to 28th. Feb. 1991
PRINCIPAL INVESTIGATOR:	Dr. John C. Gregory
INSTITUTION:	University of Alabama in Huntsville (UAH)
CO-INVESTIGATORS:	Dr. Y. Takahashi, UAH Dr. T.Hayashi, UAH C. Thoburn, UAH Dr. T. A. Parnell, MSFC Dr. J. H. Derrickson, MSFC J. W. Watts, Jr., MSFC Prof. P. H. Fowler, Univ. of Bristol, U.K. Dr. M. R. W. Masheder, Univ. of Bristol, U.K.

Background

Cosmic Ray Groups at the University of Alabama in Huntsville (UAH), Marshall Space Flight Center (MSFC) and the University of Bristol (U.K.) are collaborating in the development of the Bristol University Gas Spectrometer number 4 (BUGS 4). The BUGS 4 detector is designed to measure the charge spectrum for species between oxygen and the iron peak as a function of energy per nucleon, between 20 and 1000 GeV/amu. It is particularly concerned with energies above 50 Gev/amu. The high energy component is considerably less affected by propagation through the interstellar medium than the lower energy component and is expected to approach the original charge spectrum of the source more closely. This information allows one to unravel the effects of cosmic ray production, acceleration and propagation.

The detector consists of two concentric aluminium spheres of radii 1.0 and 1.38 meters. The inner sphere is supported by two conical webs of half angle 75°. The four regions A, B, C, and D, shown in figure 1 are thus defined. The equatorial region D is not in the detectable cosmic ray beam and is used to house the photomultipliers and electronics.

Regions A and C are Cerenkov counters each viewed by 16 photomultipliers. Region A has a 6mm thick shell of PILOT 425, which has a Cerenkov threshold of $\gamma = 1.34$. Region C has a similar shell 1.5mm thick, but is also filled with freon gas (CF_2Cl_2) which has a Cerenkov threshold of about $\gamma = 20$.

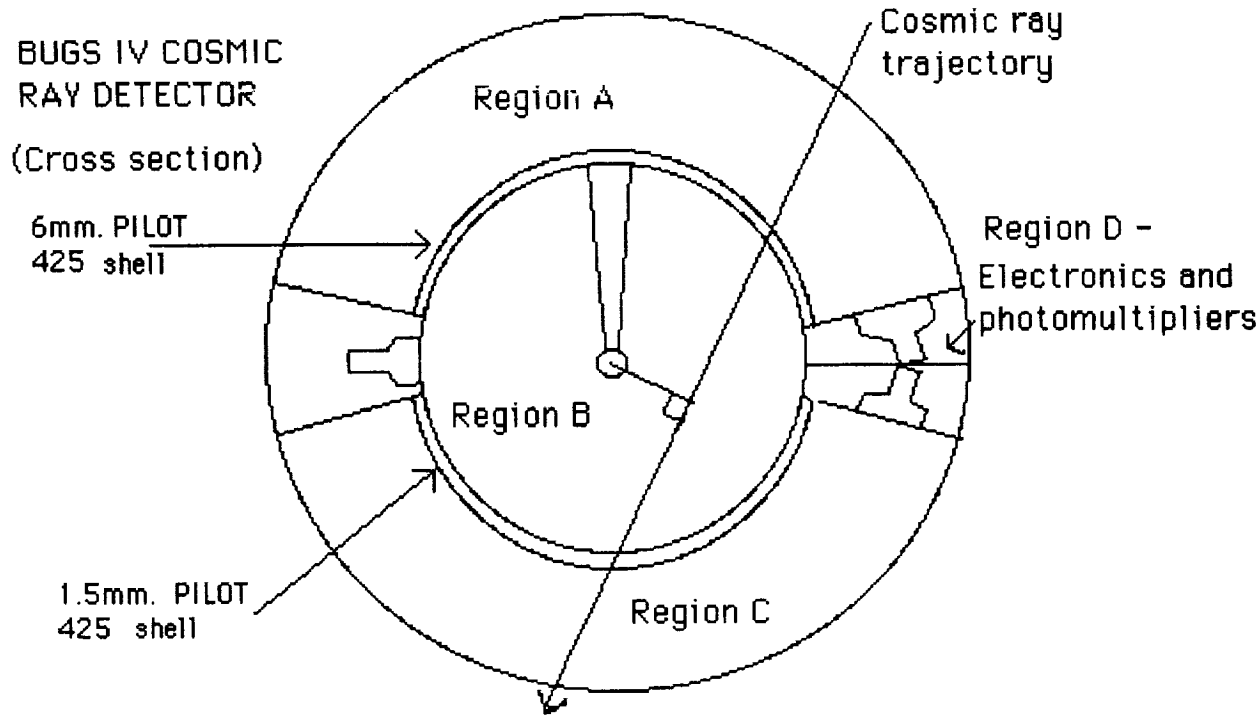

Figure 1

The central volume acts both as a scintillation counter and as a spherical drift chamber. It contains a mixture of He, Ne, Ar, and N_2. It is viewed by 8 photomultipliers fitted with wavelength shifting radiance amplifiers, which enhance the ultra-violet response down to λ = 200 nm. A 2 inch diameter electrode at the center carries a high positive voltage, the feed to this electrode is screened by a semiconducting ceramic support designed to maintain the resulting radial electric field to high precision.

The apparatus is triggered by coincident signals from regions A and C. To estimate the charge and energy of a cosmic ray we measure the light emitted by gas scintillation in the central volume; Cerenkov light in regions A and C; and the gas Cerenkov light from region B when $\gamma > 80$ Gev/amu. In order to convert these to specific light yield values we need to know the path length in each region. These are all uniquely determined by distance of closest approach to the center i.e. the impact parameter. This parameter is measured with precision by the drift chamber. Electrons liberated in the ionization of the gas by a cosmic ray then drift towards the central electrode in a time proportional to the square of the distance. Those from the edge of the chamber will take about 0.5 msecs. Once in the close vicinity of the electrode these electrons can acquire sufficient energy from the field to excite argon atoms giving rise to secondary scintillation which is detected as a second pulse by the photomultipliers. By timing the arrival of the leading edge of the drift pulse after the trigger, we can measure the impact parameter within 1 mm.

The method of estimating the charge and energy of a cosmic ray depends on the energy of the particle. Calculations and experiments lead us to expect a nearly constant charge resolution of about 0.2 charge units over the whole energy range except $4.5 < \gamma < 20$. In this band the experiment is insensitive to energy so we will need to make some assumptions about the energy of the particle that will blur the charge resolution to about 1.0 charge units.

The instrument was shipped from the U.K. in February 1990 and is now housed in the Johnson Research Center at the University of Alabama in Huntsville. After a program of refurbishment, upgrading, calibration, and completion of the flight electronics, a balloon flight of the instrument is planned for 1993.

Major tasks performed during the period of this report.

1. The University of Bristol has obtained a sheet of 0.25 inch thick PILOT 425, which will be used to manufacture a new set of radiance amplifiers for the inner region B. These amplifiers will have a modified design tailored to the specific requirements of this detector. The current radiance amplifiers were obtained from a previous experiment and contain some features which result in unnecessary light loss. Light incident upon the surface of the radiance amplifier at $\lambda < 390$ nm is absorbed by the PILOT 425 and is re-emitted isotropically at $\lambda \sim 425$ nm, which is well matched to the spectral sensitivity of the photomultipliers. A large fraction of light is trapped within

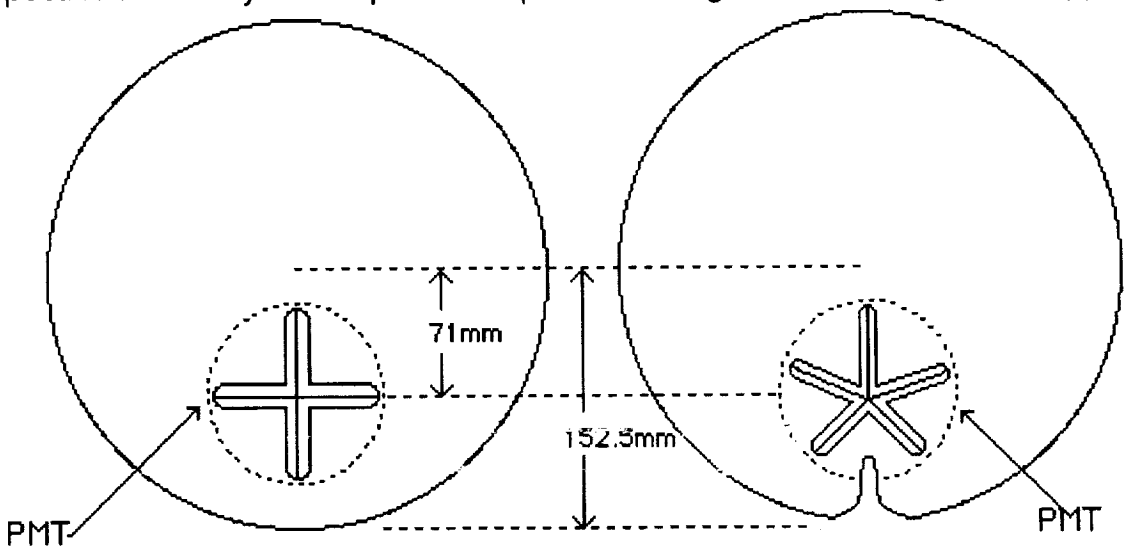

Top view of PILOT 425 radiance amplifiers.

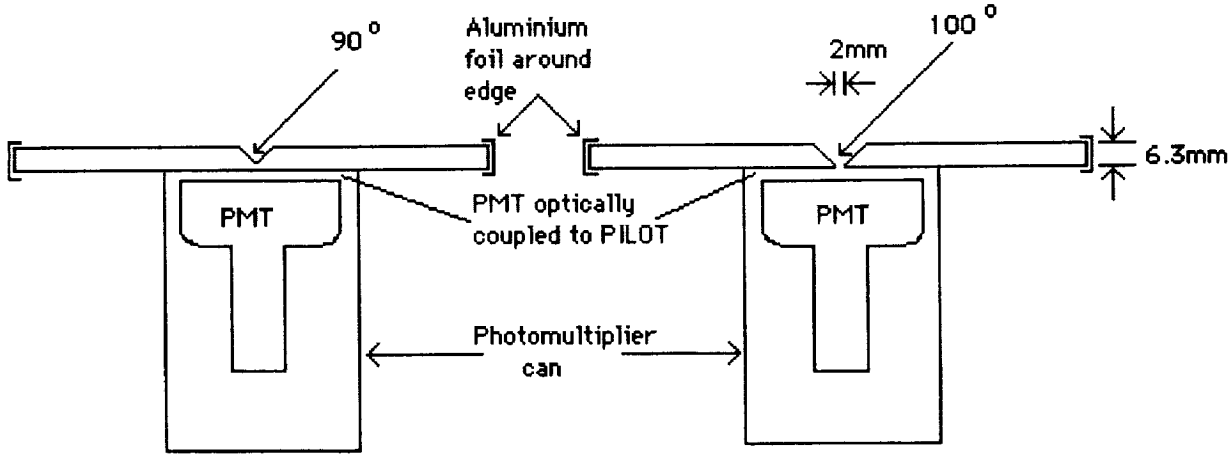

Cross section through PILOT 425 radiance amplifier.

Original design of PILOT 425 radiance amplifiers - x 4

Design of new PILOT 425 radiance amplifiers - x 6

Figure 2

the PILOT disc by total internal reflection and this light can be directed into the photomultiplier by slots milled in the PILOT above the photocathode. The design of these aerials is complete and manufacture is underway at Bristol, see figure 2 for a design comparison. The old design produced a measured 4 fold increase in signal over a bare tube. (Ref. 1) The new design should produce a 6 fold increase. (Ref. 2) As was reported in September 1990, a new set of Thorn/E.M.I. photomultiplier tubes has been selected for use in this region. Parallel development of two different base designs utilizing a positive high voltage supply continues at the University of Bristol and MSFC. Prototypes of both designs are currently being tested.

2. A system for stimulating the PILOT 425 Cerenkov elements in the upper region A was installed and used to map the light collection efficiency of the region. Light from a pulsed nitrogen laser (337nm) was directed onto the pilot shell via a fibre optic system mounted through a turntable on the top port. The signals from the 16 photomultipliers viewing this region were recorded for laser light incident at various azimuth and latitude positions on the plastic shell. Examples of the extensive data accumulated are shown in appendix A These data will be compared with a second set taken after the refurbishment of this region and with simulated values produced by software at the MSFC.

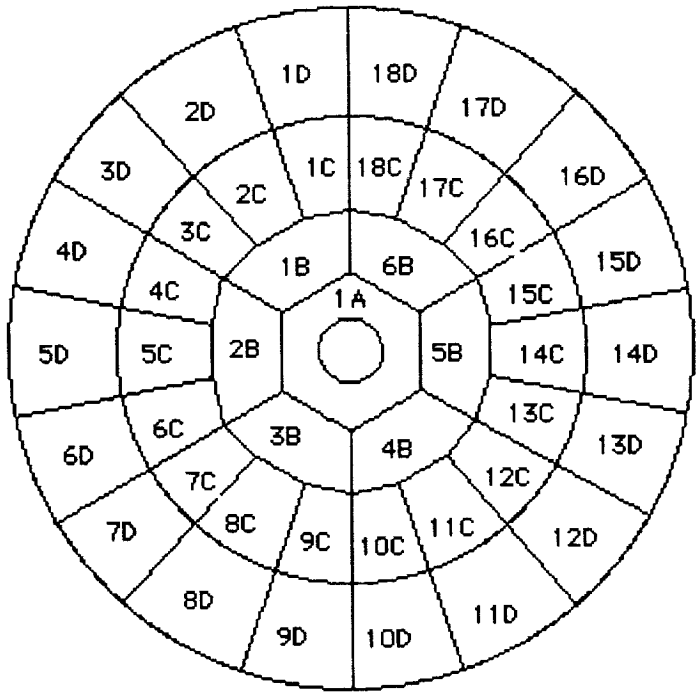

PILOT 425 TESSELLATIONS IN REGION A (viewed from above the sphere)

Figure 3

3. The upper and lower domes of the outer regions A and C have been removed. Their inner surfaces have been cleaned and repainted with Eastman-Kodak high reflectance $BaSO_4$ coating.

4. The thickness of the upper and lower PILOT 425 shells were mapped in situ using an ultra sonic thickness gage. Both shells are made up of tessellated panels (see figures 3 and 4). Several measurements were made on each panel and the whole area was measured twice. These measurements are summarized in the appendix B.

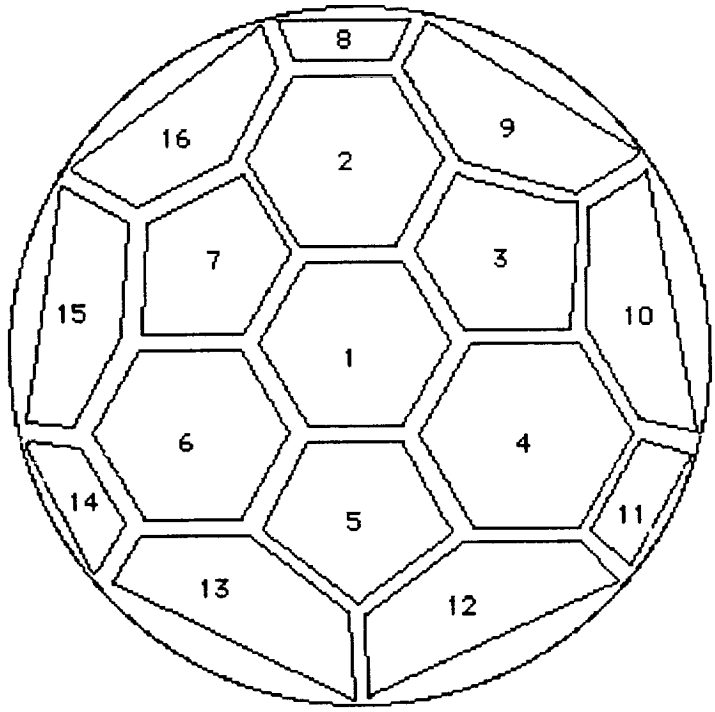

PILOT 425 TESSELLATIONS IN REGION C (viewed from underneath sphere)

Figure 4

5. Once the outer pressure vessel had been removed, a thorough inspection of the regions A and C was undertaken. An examination of the PILOT 425 shells revealed dirt and grease marks and the decision was made to remove the plastic panels to clean them. Once removed it became clear that the inner surface of the PILOT was very non-uniform, due to imperfect contact with the mould during the forming process. Since such non-uniformities could produce inhomogeneities in the emission of light from the PILOT, the inner surfaces of all the panels were frosted to a similar degree to that of the outer surface. During the close inspection of the plastic panels some non-uniformity in their wavelength shifting ability was also observed. A test system was set up in a white box, using a pulsed nitrogen laser to stimulate each panel in turn and a photomultiplier to measure the light output from each panel. These tests revealed that while all the plastic panels in region A and most of the panels in region C had a similar

efficiency, 3 panels in the lower region C did appear to be degraded. They appeared yellow in color, especially at the edges of the panel. Investigation into the method used at Bristol to heat mould the panels indicates that oven temperature and baking time may not have been rigidly controlled. We have initiated further oven tests at UAH using small samples of PILOT 425 to discover if this is indeed the cause. The positions of these "bad" panels has been noted, so if necessary we can exclude any events passing through them, although it should be possible to recalibrate on the iron peak for this subset of the data. We are investigating the possibility of replacing these "bad" panels. While the timetable makes this unlikely prior to the first balloon flight, we should be ready to optimise the detector should a second flight be approved.

6. After frosting and cleaning, the PILOT panels from region C were remounted and measurements were taken on their relative positions. The pressure transducer, damaged during the dismantling, was replaced with a spare. Region C was then reassembled.

7. The plastic panels from region A were removed so that their inner surfaces could be frosted. Once uncovered it became obvious that the white reflectance paint on the outer surface of the inner sphere in region A was very dirty. The dirt and top layers of paint were brushed off and a layer of fresh $BaSO_4$ paint was sprayed over this area. The PILOT panels from region A were frosted, cleaned, and remounted. Region A was reassembled after measurements were taken on the relative positions of the panels.

8. A trial assembly of the landing frame was carried out in December with the assistance of a mechanical engineer from Bristol. Apart from a few missing brackets, the frame is complete. The missing brackets are currently under construction in the UAH workshop.

9. Elements of the gas filling system continue to be assembled. The large volume Edwards vacuum pump has been refurbished and modified to operate with a US mains supply.

10. Progress on the flight electronics is reported by Bob Austin (MSFC) in appendix C.

Year Two Plans.

1. Complete reassembly of region A.

2. Install central drift probe.

3. Repeat mapping of light-gathering inhomogeneities in region A with fiber-optic scanning system.

4. Performance of gas scintillation and drift studies in the central detector.

5. Build, test and install amplifiers for the 32 photomultipliers in regions A and C.

6. Assemble 8 new photomultiplier systems for region B, complete with new radiance amplifiers and PMT bases.

7. Integration of the new flight electronics into the system. Testing of electronics system with the detector. Testing of the GSE.

8. Testing of assembled instrument.

9. Verification of mechanical analysis and tests of the support system.

10. Continuation of the detector performance simulations.

11. Fabrication of new PILOT 425 tessellations for region C and tests on heat degradation of the plastic.

12. Software production for flight system (coordination with MSFC)

13. Software production for GSE (coordination with MSFC)

References.

1. Swordy, S.P., PhD Thesis, University of Bristol, 1979

2. Fowler, P.H., Private Communication, 1991

Chris Thoburn
1st May 1991

APPENDIX A

Figures 5 and 6 show the orientation of the fibre system used to stimulate the PILOT 425 plastic shell of region A and the positions of the 16 photomultiplier tubes in azimuth.

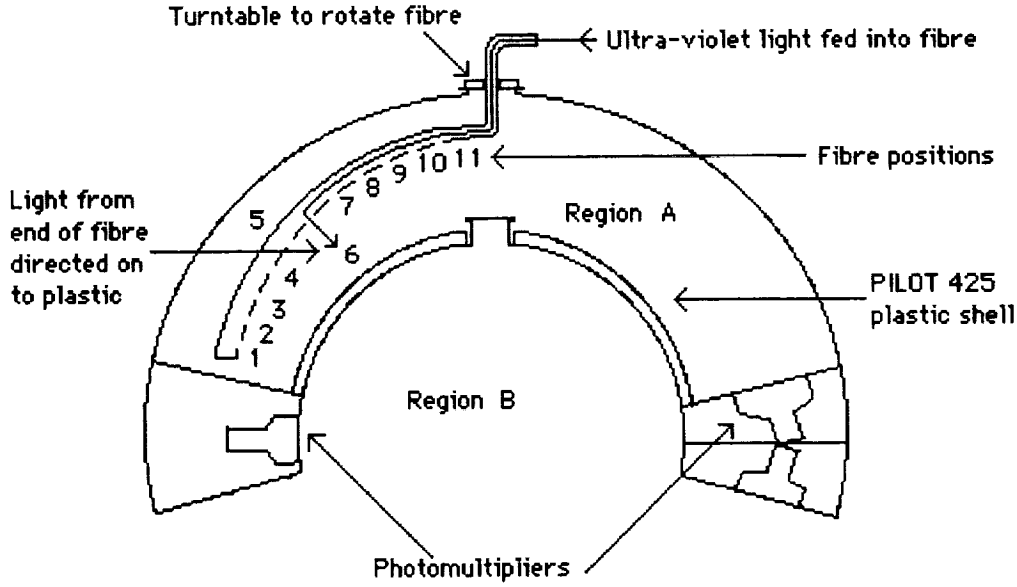

CROSS SECTION OF REGION A FIBRE SYSTEM

Figure 5

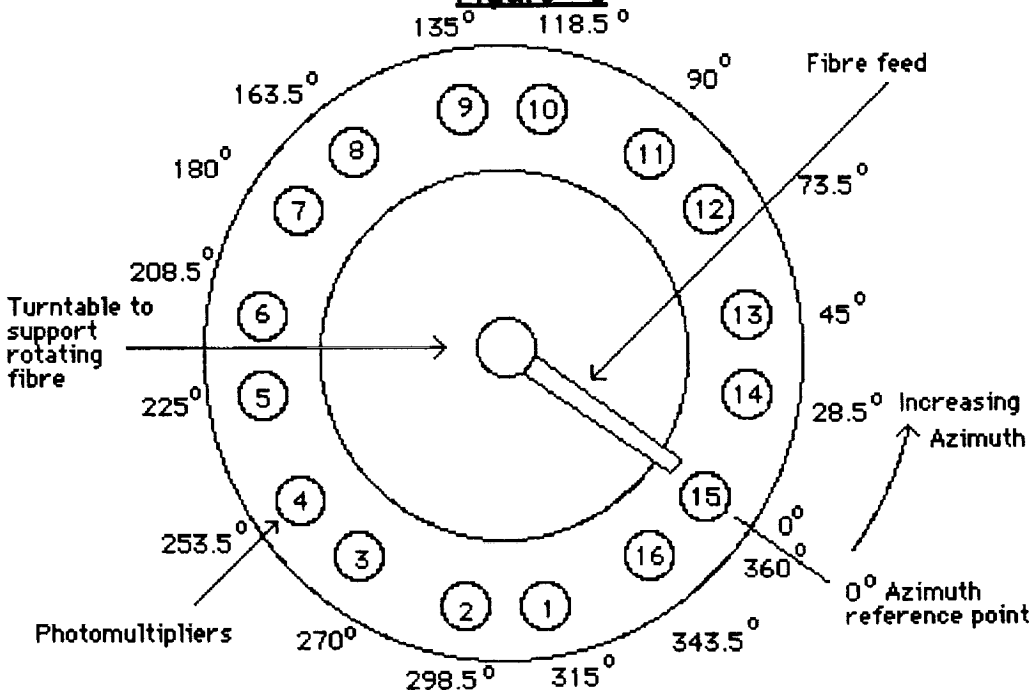

PLAN VIEW OF REGION A FIBRE SYSTEM

Figure 6

The PILOT 425 was stimulated by an ultra-violet source positioned at various azimuth angles around the sphere. A nitrogen laser was used as the source of light with λ = 337nm, unfortunately the photomultipliers can detect light at this wavelength directly. The signal from each of the 16 photomultipliers viewing the region was recorded for each stimulated point. Due to limitations on the high voltage supply to the photomultipliers, no corrections could be made for individual tube gain. Eleven complete azimuthal revolutions were sampled at different latitude settings. Fibre position 11 being closest to the pole and position 1 being closest to the equator. We were unable to take measurements with all 16 tubes at all fibre positions and azimuths due to time restrictions. The apparent drift in photomultiplier tube position with latitude is due to the fibre light feed twisting as the latitude is increased, directing the light to a slightly different point on the PILOT surface.

Figures 7 to 10 show the variation in the signal from photomultiplier 2 with fibre position (i.e. latitude) for all azimuth positions. The signals were measured at 10 degree intervals in azimuth. PMT number 2 is at an azimuth of 298.5°. These results show the twist in the fibre at positions greater than 4, which allowed direct light to fall onto the photocathode.

Figures 11 to 14 show the signal response from photomultipliers 2, 6, 10 and 14. These 4 tubes were at 90° separation. Each figure shows the response at a different fibre position i.e. latitude.

Figures 15 to 18 show the average of the signals from all the photomultipliers sampled at each azimuth setting, for fibre positions 1, 4, 8 and 11. 15 of the 16 tubes were sampled at position 1; PMT 15 was removed to investigate a tube base problem. Only the even numbered tubes were sampled at position number 4. Opposite pairs of tubes were sampled at positions 8 and 11, i.e. PMTs 1, 2, 5, 6, 9, 10, 13, and 14. As expected the ratio of peak to background signal decreases as latitude increases, requiring multiple reflections for light to reach the tube.

Figure 7

PMT 2 AT 0-90 DEGREES

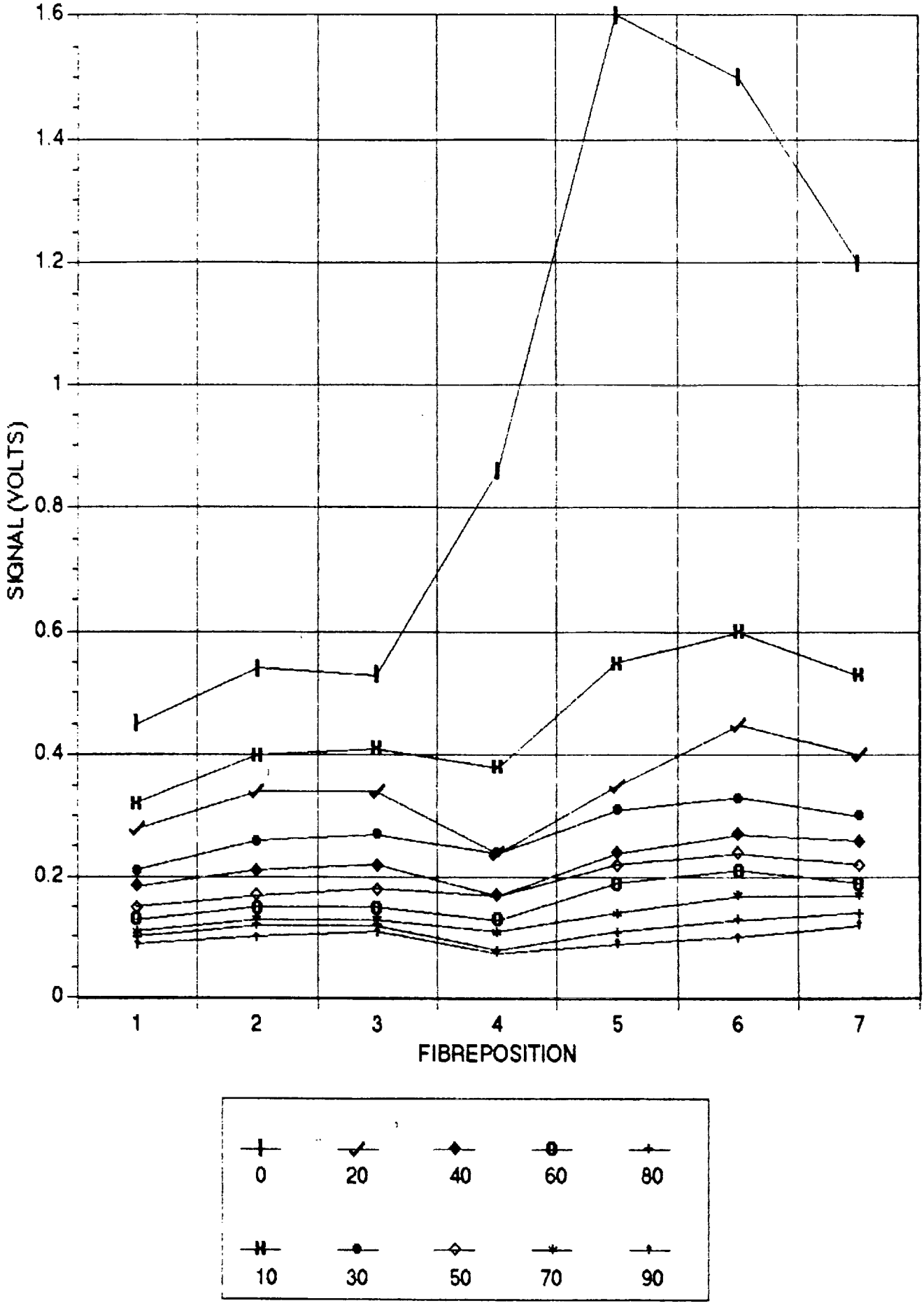

Figure 8

PMT 2 AT 100-180 DEGREES

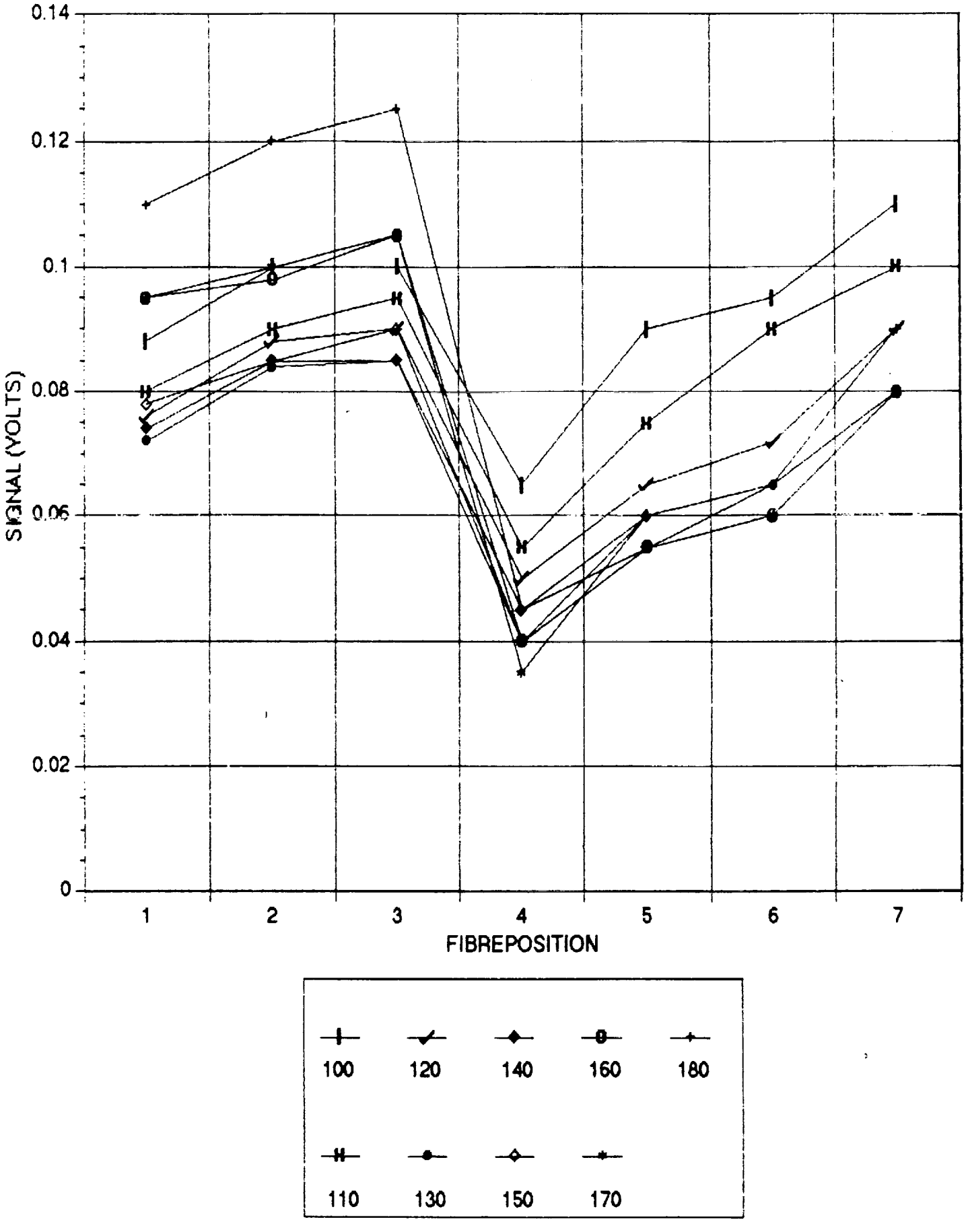

Figure 9

PMT 2 AT 190-270 DEGREES

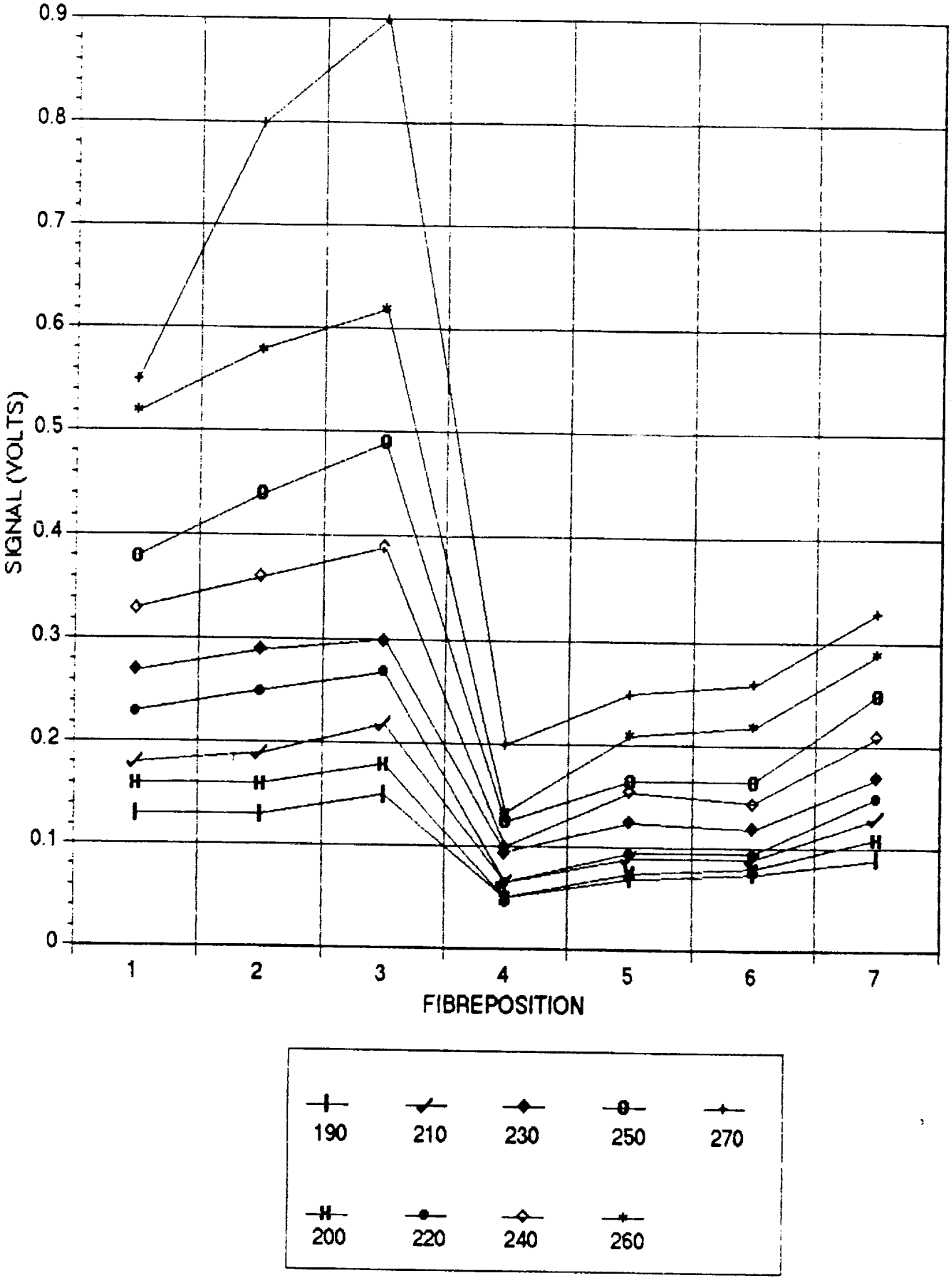

Figure 10

PMT 2 AT 280-360 DEGREES

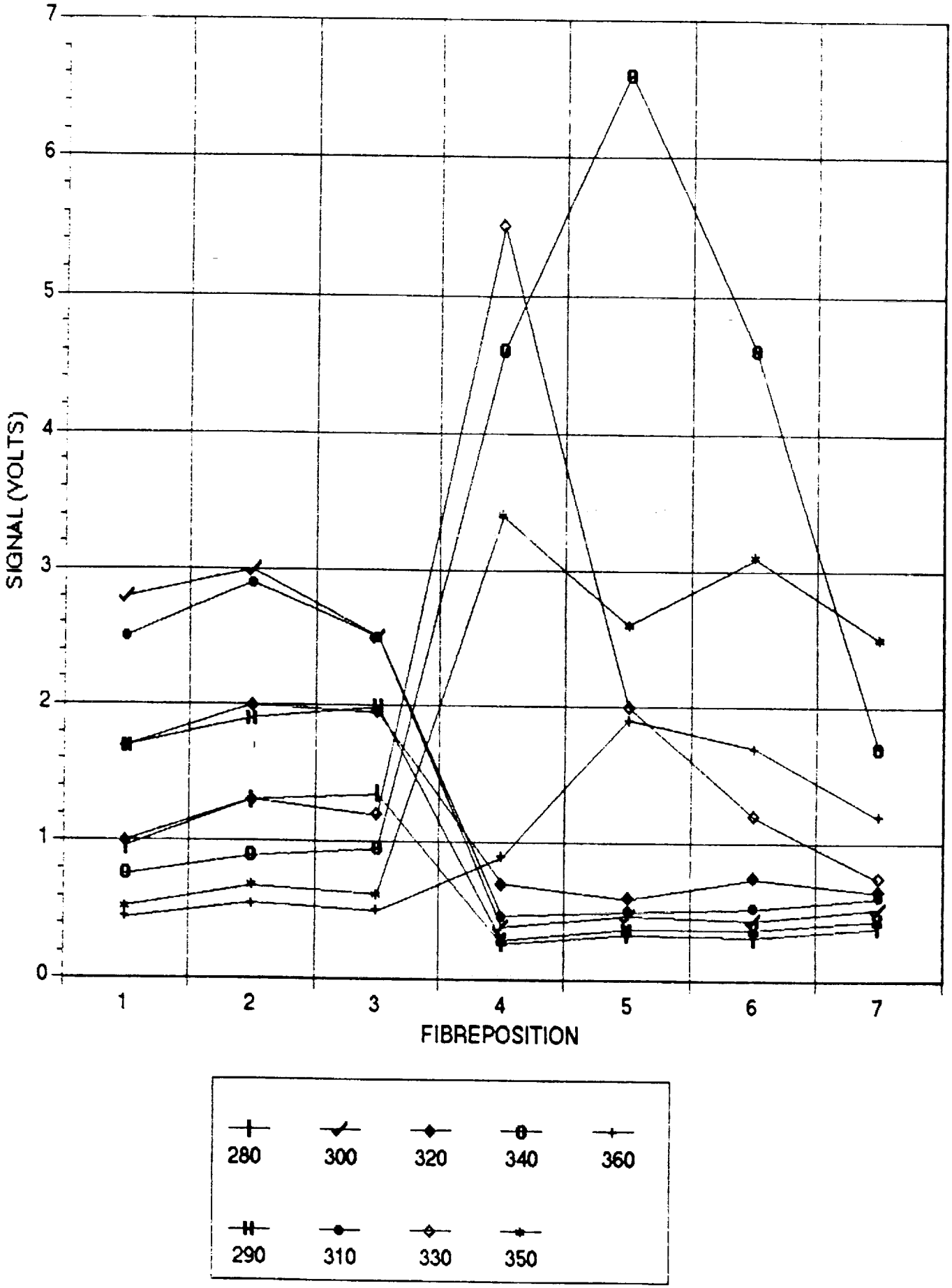

Figure 11

PMTs 2, 6, 10 and 14 v. Azimuth Degrees
For fibre position number 1

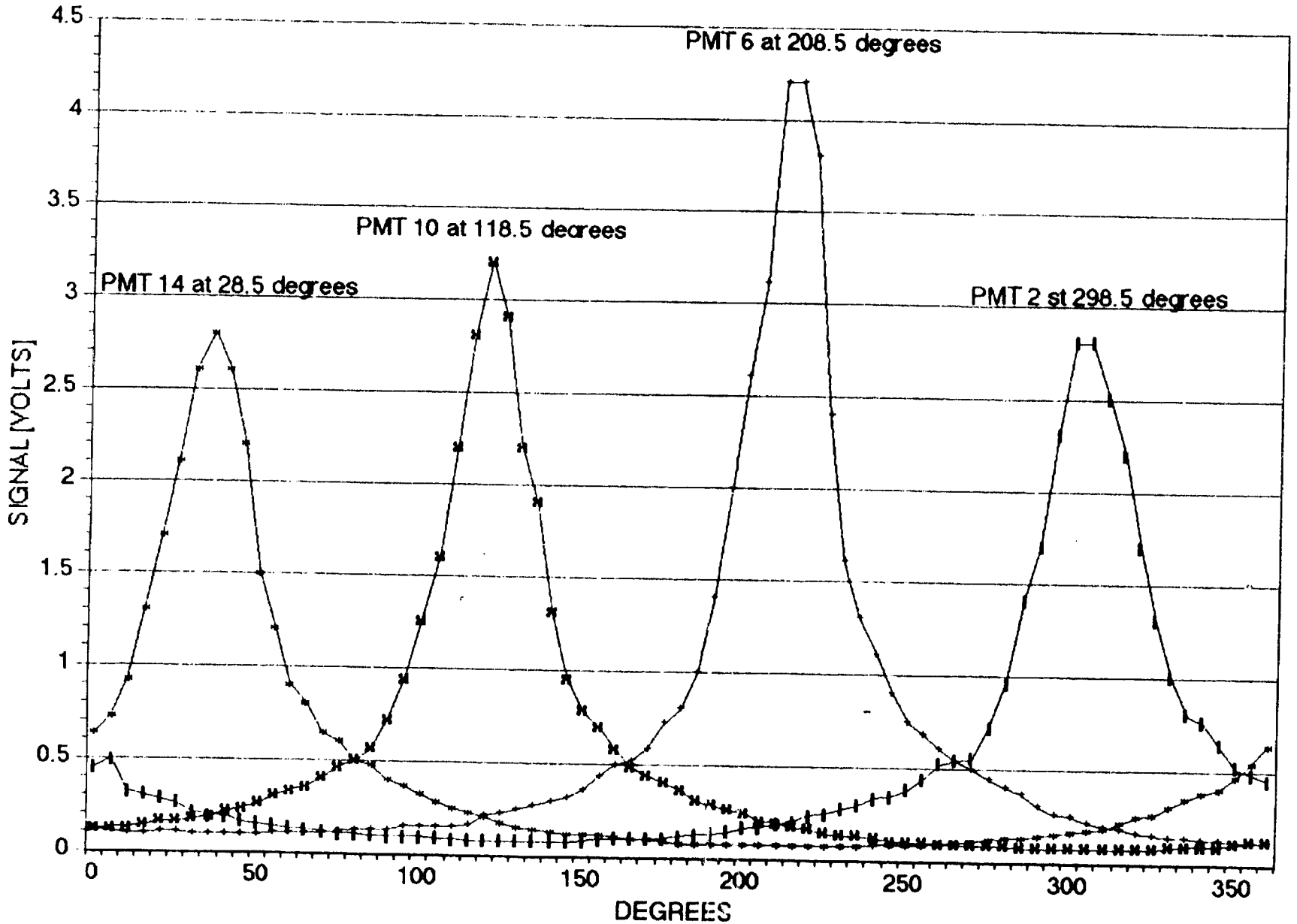

Figure 12

PMTs 2, 6, 10 and 14 v. Azimuth Degrees
For fibre position number 4

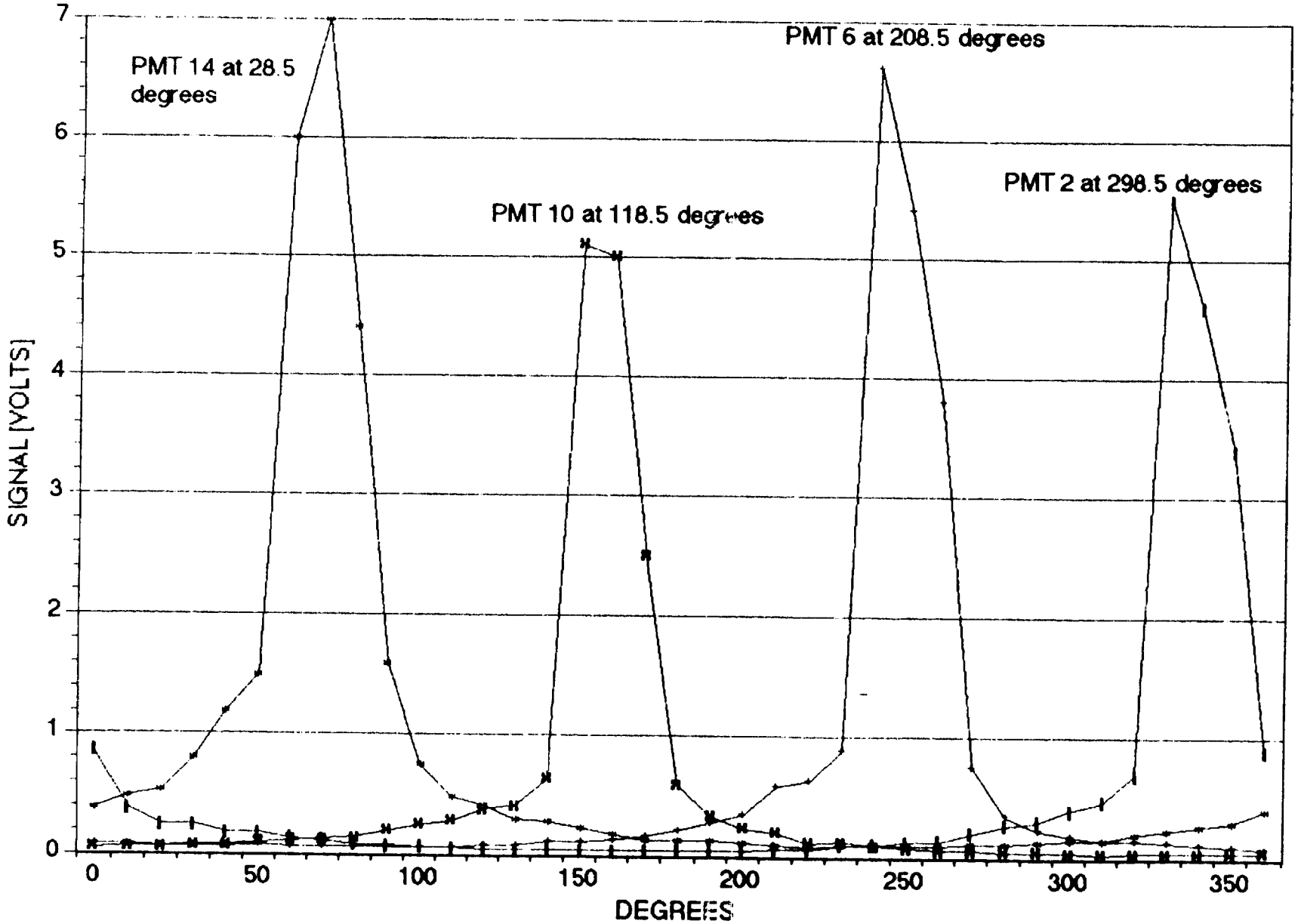

Figure 13

PMTs 2, 6, 10 and 14 v. Azimuth Degrees
For fibre position number 8

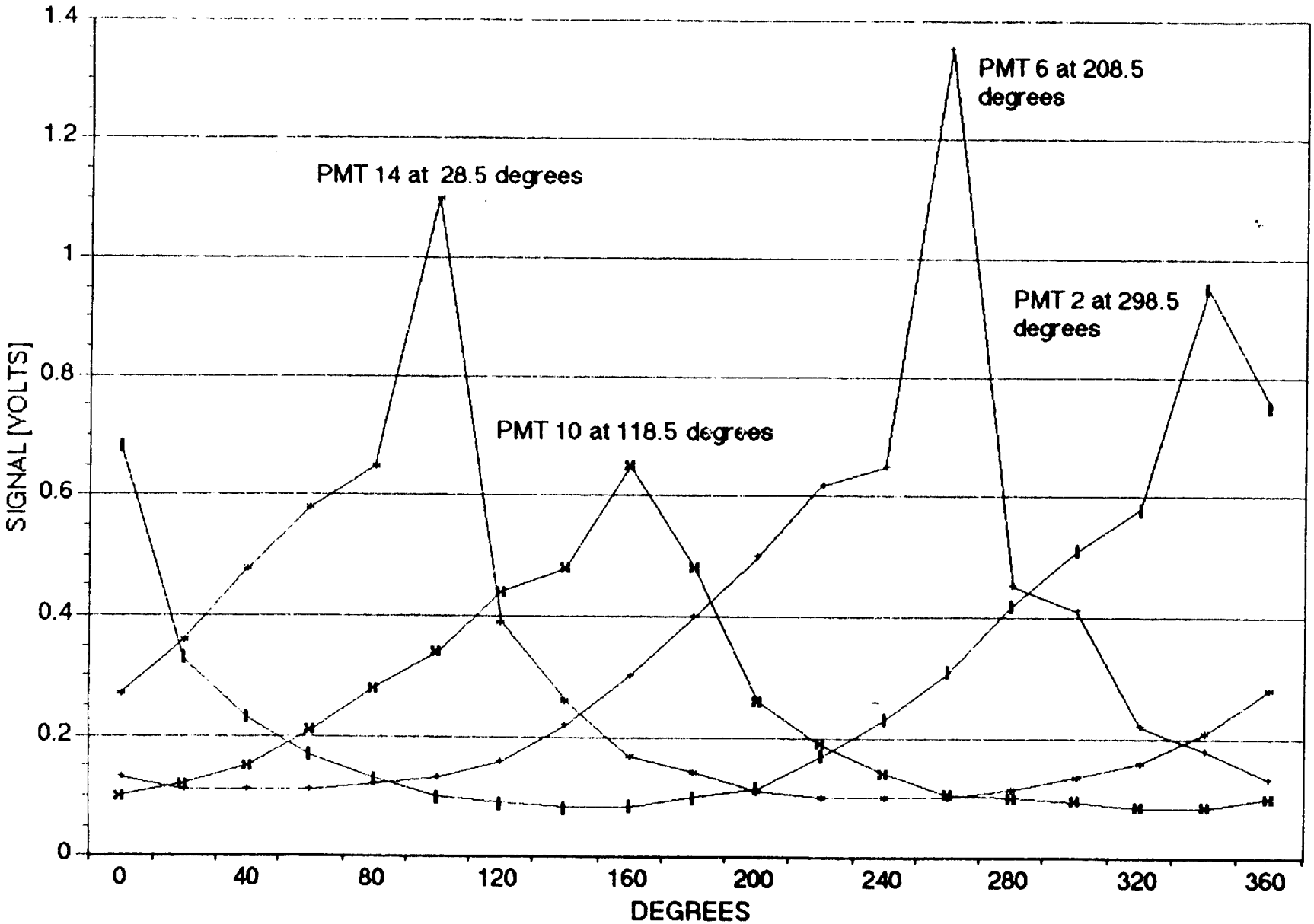

Figure 14

PMTs 2, 6, 10 and 14 v. Azimuth Degrees
For fibre position number 11

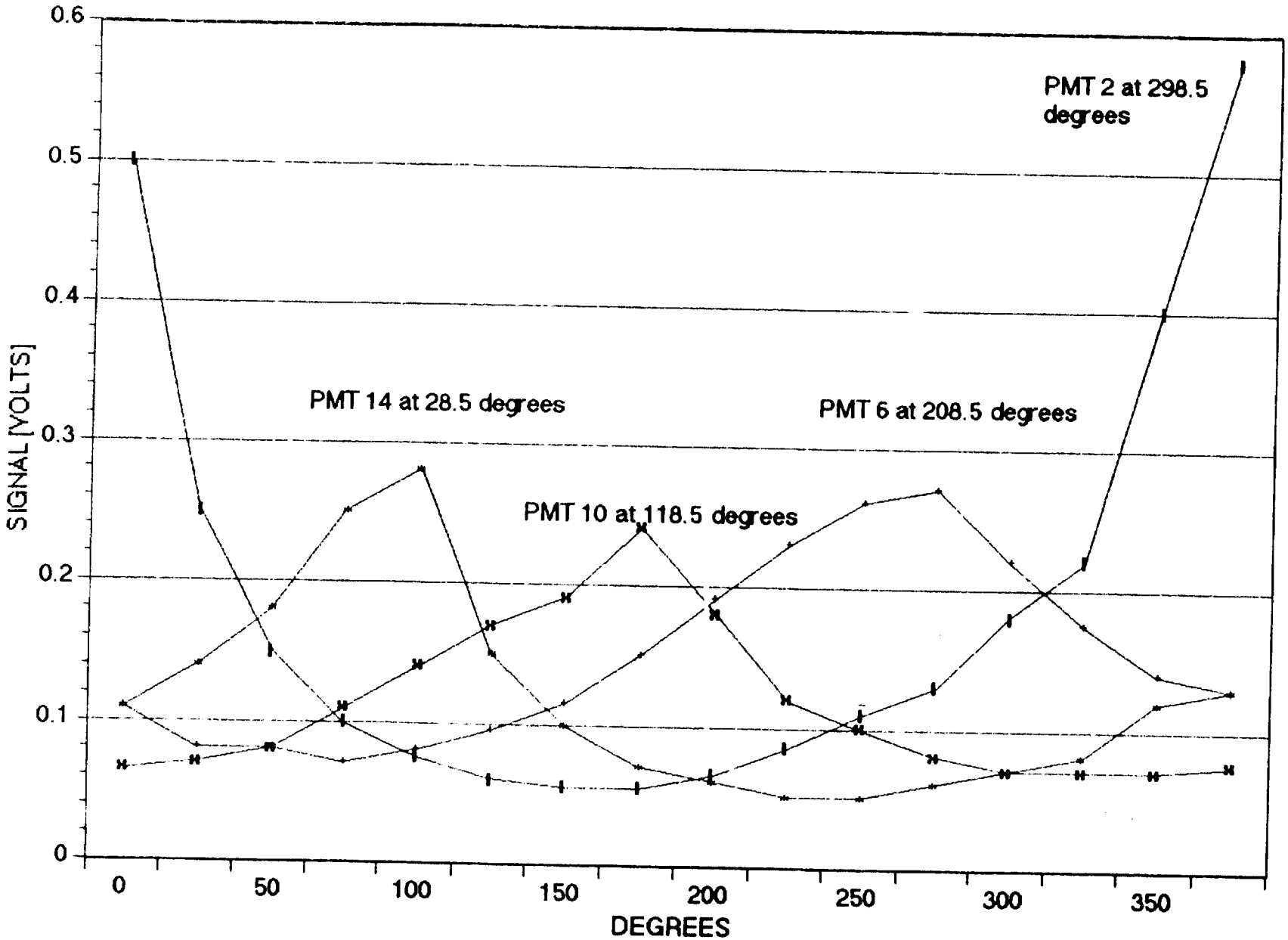

Figure 15

Average of all PMTs for all azimuths at fibre position number 1

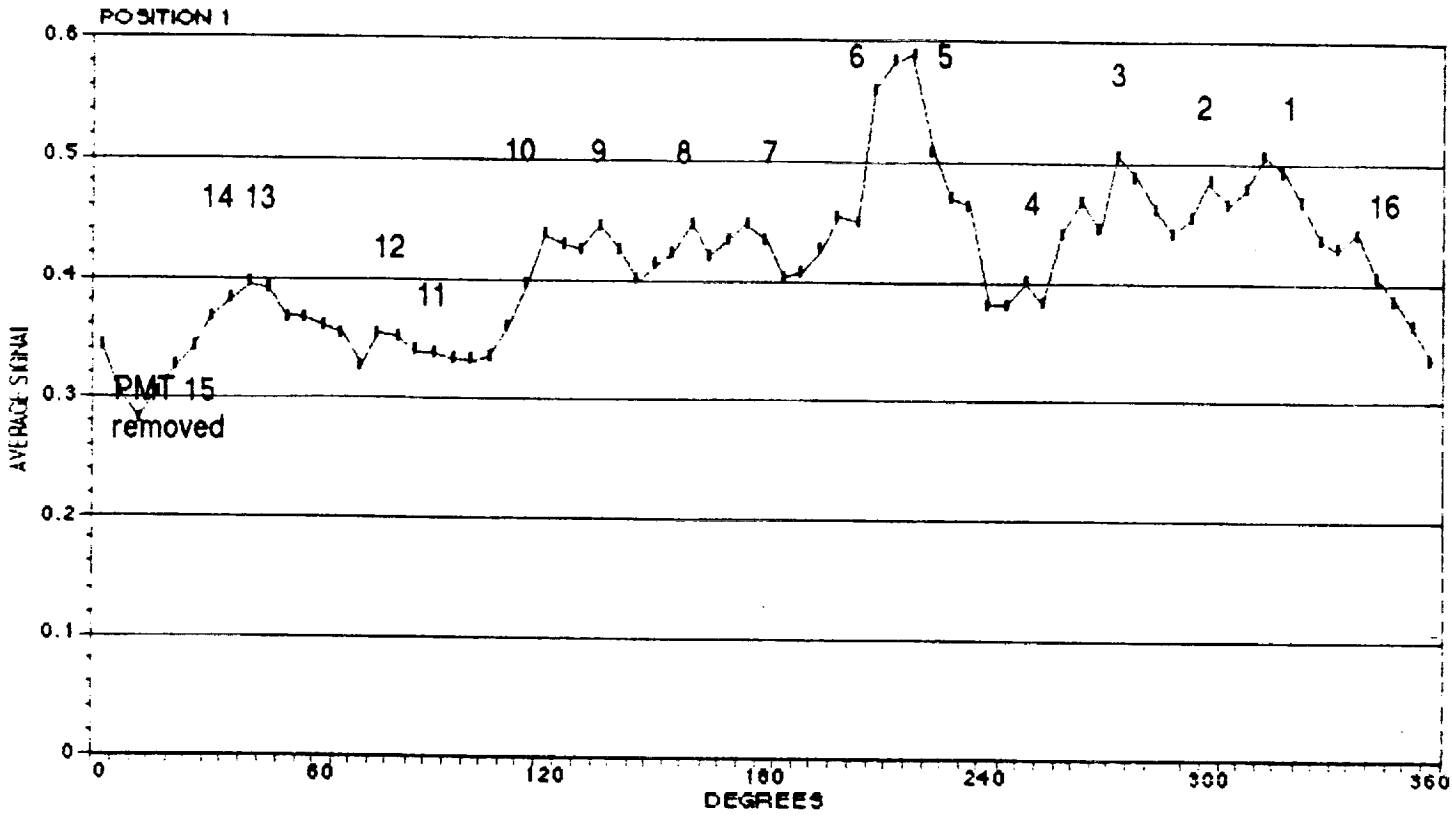

Figure 16

Average of all PMTs for all azimuths at fibre position number 4

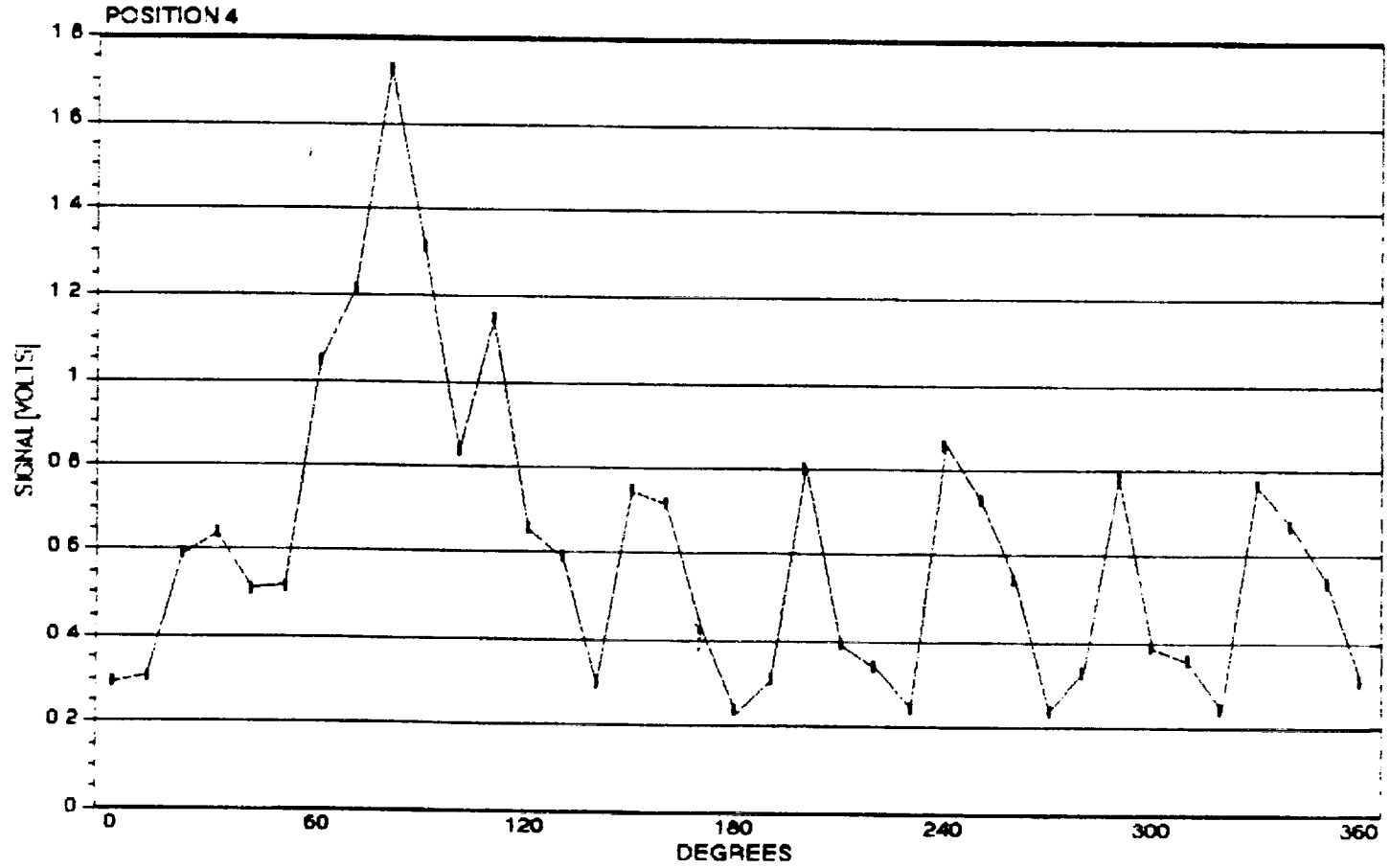

Figure 17

Average of all PMTs for all azimuths at fibre position number 8

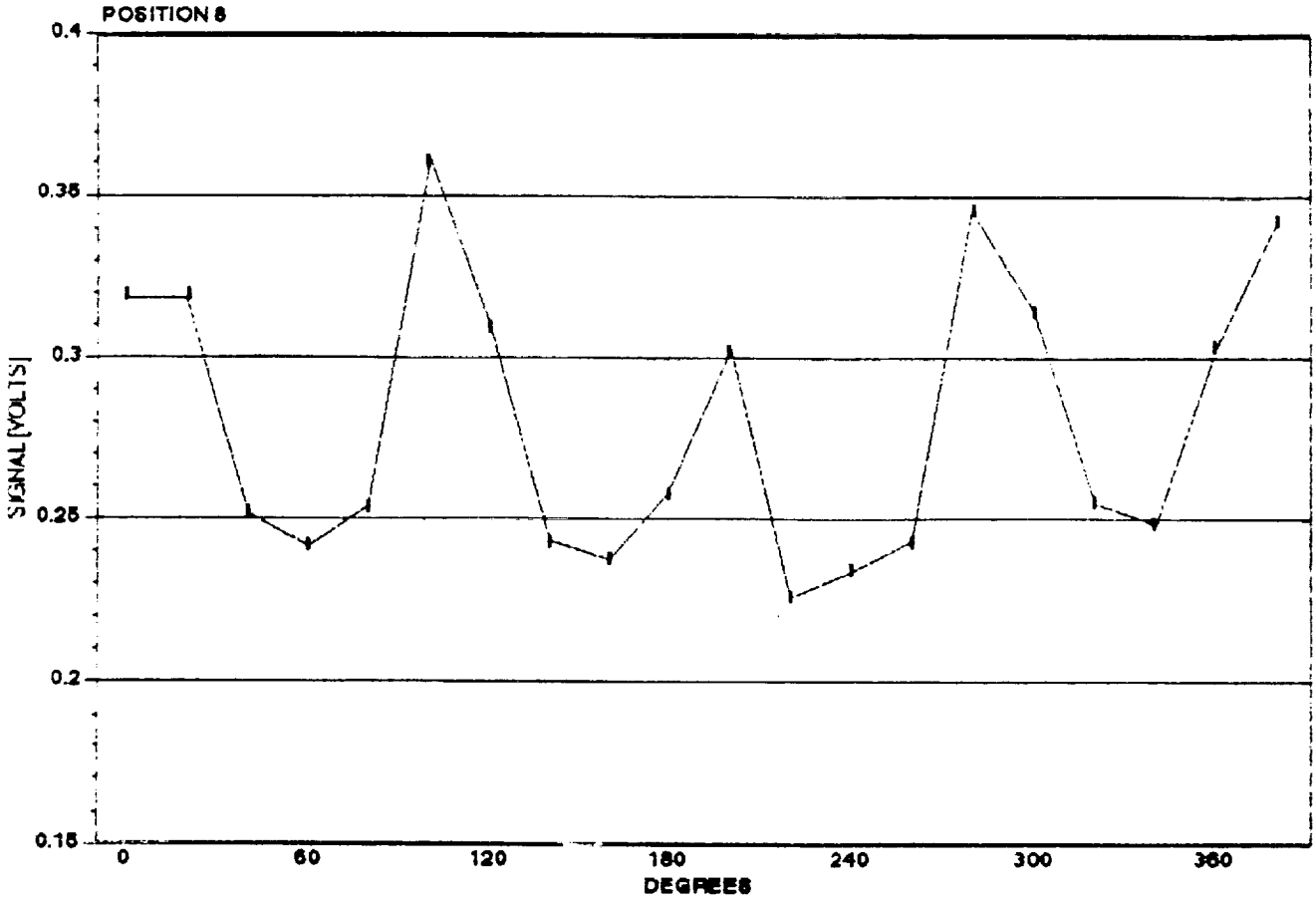

Figure 18

Average of all PMTs for all azimuths at fibre position number 11

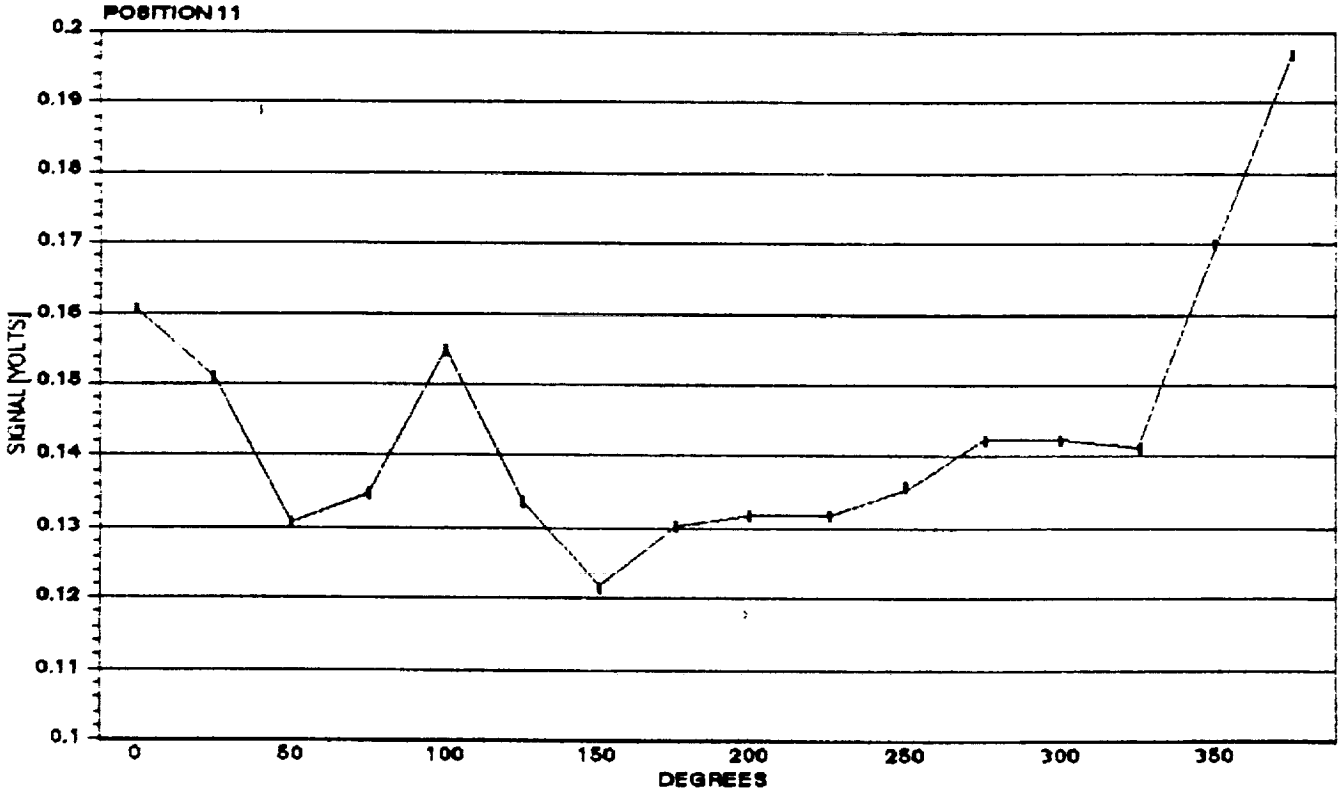

APPENDIX B

These measurements were made with a Panametrics ultra-sonic thickness gage, while the panels were mounted onto the inner sphere of the detector. Glycerin was used to couple the detector to the surface of the PILOT 425. The gage was calibrated for the velocity of sound in PILOT using a sample of known thickness. All the measurements in this appendix are quoted in mm.

THICKNESS OF PILOT 425 PANELS IN REGION A

First set of measurements:

PANEL NUMBER	MEAN THICK. OF PANEL	STANDARD DEVIATION	MAX. THICK. OF PANEL	MIN. THICK. OF PANEL
1A	5.795	0.021	5.843	5.755
1B	5.816	0.045	5.868	5.721
2B	5.788	0.041	5.893	5.727
3B	5.792	0.04	5.881	5.738
4B	5.796	0.049	5.867	5.716
5B	5.827	0.047	5.883	5.723
6B	5.791	0.037	5.852	5.723
1C	5.784	0.033	5.818	5.721
2C	5.809	0.051	5.888	5.734
3C	5.794	0.049	5.873	5.706
4C	5.785	0.019	5.816	5.756
5C	5.845	0.049	5.93	5.744
6C	5.81	0.043	5.866	5.725
7C	5.816	0.036	5.858	5.738
8C	5.793	0.044	5.869	5.718
9C	5.834	0.053	5.89	5.746
10C	5.832	0.022	5.86	5.79
11C	5.822	0.054	5.92	5.746
12C	5.808	0.034	5.882	5.747
13C	5.823	0.041	5.885	5.765
14C	5.77	0.032	5.813	5.718
15C	5.797	0.042	5.853	5.713
16C	5.764	0.033	5.81	5.712
17C	5.802	0.029	5.852	5.744
18C	5.805	0.033	5.85	5.73
1D	5.796	0.056	5.869	5.66
2D	5.811	0.043	5.857	5.705
3D	5.784	0.092	5.881	5.59
4D	5.791	0.054	5.866	5.698
5D	5.782	0.079	5.894	5.637

PANEL NUMBER	MEAN THICK. OF PANEL	STANDARD DEVIATION	MAX. THICK. OF PANEL	MIN. THICK. OF PANEL
6D	5.8	0.075	5.922	5.658
7D	5.754	0.055	5.823	5.633
8D	5.76	0.06	5.851	5.662
9D	5.844	0.043	5.908	5.766
10D	5.686	0.087	5.816	5.55
11D	5.747	0.034	5.782	5.688
12D	5.76	0.057	5.822	5.642
13D	5.8	0.059	5.873	5.719
14D	5.813	0.035	5.866	5.763
15D	5.8	0.052	5.889	5.72
16D	5.812	0.036	5.867	5.743
17D	5.802	0.068	5.884	5.698
18D	5.759	0.08	5.899	5.643

Velocity of sound used during this set of measurements: 2.725 mm/μsec.

Mean value of thickness over whole of region A: 5.795
Standard deviation: 0.057
Maximum value over whole region A: 5.93
Minimum value over whole region A: 5.55

Second set of measurements:

PANEL NUMBER	MEAN THICK. OF PANEL	STANDARD DEVIATION	MAX. THICK. OF PANEL	MIN. THICK. OF PANEL
1A	5.789	0.02	5.833	5.753
1B	5.815	0.043	5.865	5.746
2B	5.803	0.033	5.882	5.756
3B	5.797	0.033	5.868	5.741
4B	5.794	0.041	5.856	5.732
5B	5.824	0.047	5.893	5.743
6B	5.79	0.024	5.844	5.759
1C	5.775	0.045	5.843	5.684
2C	5.814	0.037	5.886	5.766
3C	5.798	0.034	5.849	5.732
4C	5.751	0.079	5.846	5.549
5C	5.845	0.054	5.908	5.742
6C	5.82	0.055	5.914	5.699
7C	5.83	0.049	5.885	5.75
8C	5.821	0.057	5.899	5.735
9C	5.866	0.038	5.909	5.795
10C	5.86	0.033	5.897	5.806
11C	5.868	0.046	5.933	5.782

PANEL NUMBER	MEAN THICK. OF PANEL	STANDARD DEVIATION	MAX. THICK. OF PANEL	MIN. THICK. OF PANEL
12C	5.831	0.039	5.897	5.762
13C	5.865	0.054	5.939	5.79
14C	5.805	0.036	5.863	5.746
15C	5.82	0.053	5.901	5.748
16C	5.798	0.034	5.835	5.743
17C	5.832	0.032	5.886	5.784
18C	5.829	0.021	5.881	5.808
1D	5.781	0.062	5.838	5.643
2D	5.78	0.048	5.833	5.687
3D	5.761	0.105	5.896	5.547
4D	5.772	0.036	5.814	5.694
5D	5.778	0.082	5.896	5.63
6D	5.784	0.077	5.861	5.634
7D	5.76	0.073	5.853	5.621
8D	5.773	0.053	5.852	5.688
9D	5.843	0.038	5.894	5.781
10D	5.719	0.1	5.87	5.573
11D	5.762	0.035	5.799	5.698
12D	5.778	0.06	5.852	5.654
13D	5.811	0.055	5.876	5.719
14D	5.814	0.043	5.893	5.763
15D	5.796	0.071	5.908	5.699
16D	5.829	0.038	5.884	5.779
17D	5.82	0.053	5.907	5.736
18D	5.776	0.07	5.885	5.664

Velocity of sound used during this set of measurements: 2.749 mm/μsecs.

Mean value of thickness over whole of region A: 5.804
Standard deviation: 0.062
Maximum value over whole region A: 5.939
Minimum value over whole region A: 5.547

THICKNESS OF PILOT 425 PANELS IN REGION C

First set of measurements:

PANEL NUMBER	MEAN THICK. OF PANEL	STANDARD DEVIATION	MAX. THICK. OF PANEL	MIN. THICK. OF PANEL
1	1.345	0.043	1.409	1.229
2	1.36	0.027	1.466	1.33
3	1.393	0.029	1.464	1.342
4	1.381	0.03	1.486	1.32
5	1.398	0.03	1.457	1.35
6	1.366	0.019	1.403	1.317
7	1.375	0.022	1.428	1.33
8	1.324	0.052	1.415	1.27
9	1.443	0.052	1.541	1.363
10	1.417	0.043	1.494	1.349
11	1.393	0.039	1.481	1.354
12	1.36	0.06	1.448	1.224
13	1.369	0.033	1.432	1.311
14	1.422	0.032	1.472	1.39
15	1.382	0.034	1.457	1.327
16	1.377	0.039	1.442	1.282

Velocity of sound used during this set of measurements: 2.725 mm/μsecs.

Mean value of thickness over whole of region A:	1.345
Standard deviation:	0.043
Maximum value over whole region A:	1.409
Minimum value over whole region A:	1.229

Second set of measurements:

PANEL NUMBER	MEAN THICK. OF PANEL	STANDARD DEVIATION	MAX. THICK. OF PANEL	MIN. THICK. OF PANEL
1	1.348	0.041	1.415	1.232
2	1.385	0.023	1.462	1.337
3	1.399	0.034	1.47	1.343
4	1.381	0.024	1.438	1.327
5	1.411	0.03	1.469	1.343
6	1.374	0.027	1.469	1.317
7	1.383	0.019	1.415	1.339
8	1.319	0.053	1.409	1.264
9	1.46	0.054	1.555	1.393
10	1.418	0.043	1.497	1.351

PANEL NUMBER	MEAN THICK. OF PANEL	STANDARD DEVIATION	MAX. THICK. OF PANEL	MIN. THICK. OF PANEL
11	1.396	0.027	1.421	1.348
12	1.357	0.065	1.462	1.204
13	1.38	0.039	1.459	1.321
14	1.417	0.052	1.499	1.323
15	1.398	0.032	1.482	1.351
16	1.381	0.028	1.442	1.342

Velocity of sound used during this set of measurements: 2.749 mm/μsecs.

Mean value of thickness over whole of region A:	1.386
Standard deviation:	0.044
Maximum value over whole region A:	1.555
Minimum value over whole region A:	1.204

APPENDIX C

BUGS BALLOON FLIGHT DATA SYSTEM and GSE PROGRESS REPORT

Progress has been made in several areas of the BUGS balloon flight instrument electronics and GSE. These areas are:

1. Drift Pulse Digitizer and associated data system

The digitizer for the 500 μsecond duration drift pulse has been successfully breadboarded and tested. The system produces a twelve bit word representing the input signal level each μsecond. This digitizer is designed to be operated with its reference elevated to the PMT anode potential in order to accomplish DC coupling to the anode signal. A sixteen MHz clock is passed to each of the eight digitizers via fiber optic cables. The resulting data stream is also returned from each digitizer via fiber optic cables.

Synchronization of the digitizers to each event is accomplished by simultaneously gating the 16 MHz clock to each digitizer when a trigger event has been seen. This appearance of the clock at the digitizer generates an immediate reset and convert command in each of the eight digitizers. The first valid result returns as the second word received from the digitizers. This word represents the signal amplitude seen at the ADC's sample and hold input 62.5 nsecs. (-0 : +62.5nsecs.) after the trigger signal is sent to the clock generator. Once the required 500 events have been collected, the 16MHz clock is terminated until another trigger is seen.

The rapid burst of 4000 data words (500 x 8) will be received in a first in first out (FIFO) register. This register will then be unloaded to telemetry along with the peak sensing ADC outputs and a subset of the housekeeping data. The telemetry rate is 156KBPS. Each event will take approximately 0.3 seconds to telemeter unless some data compression is used.

2. Parts Procurement

The following orders have been received:

Amptek A250 charge sensitive preamps	3
Analog Devices AD9003 ADC	3
Gateway 80486 GSE computer	1
Dynatem 68030 VME processor	1
Dynatem Dana12 VME housekeeping ADC	1

The following items are on order and due in:

LeCroy 2249 12 CH 11 bit pulse ADCs	4
Kenetic Sys Crate Ctrlr 3922	1
Kenetic Sys FIFO 3842-J4D	1
Kenetic Sys CAMAC/VME I/F 2917	1
Power General DC/DC converters	10

The following items have been recently ordered:

Hewlett Packard fiber optic TX, RX and cables	10 sets

The following items are in stock:

Kepco high efficiency DC/DC converters	AR
CAMAC crate	1

The following items are to be ordered:

Additional quantities of Amptek preamps
Additional quantities of Analog Devices AD 9003

3. High Voltage Power Supply

EB12 has placed on order the parts necessary to fabricate 40 programmable negative high voltage power supplies and 10 positive high voltage power supplies. The supplies are based on the BATSE power supply designs and are remotely programmable via serial link.

Tasks remaining

The Amptek preamps are to be mated with the ADC and that combination mated with the PMTs.

A programmable current source is being developed to pulse an LED as a simulation of the inner detector drift pulse signal.

A printed circuit board is to be designed that integrates the preamp, digitizer, and fiber optic links into the PMT housings.

The entire coincidence, gating, and clock drive system must be designed and built.

The entire flight software program must be written.

The entire GSE software program must be written.

ES62/Austin
26th. February 1991.

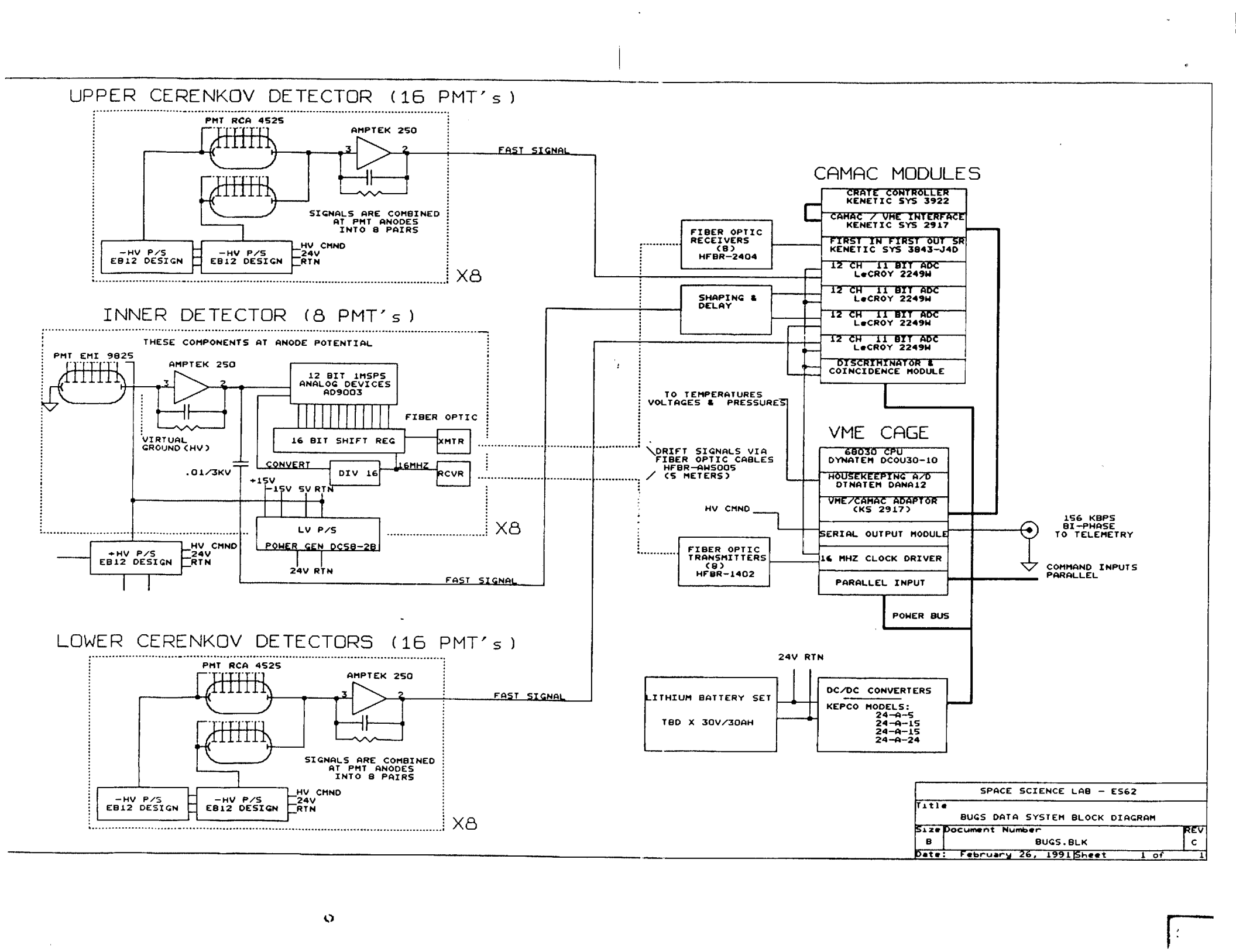
UPPER CERENKOV DETECTOR (16 PMT's)
PMT RCA 4525
AMPTEK 250
FAST SIGNAL
SIGNALS ARE COMBINED AT PMT ANODES INTO 8 PAIRS
-HV P/S EB12 DESIGN
-HV P/S EB12 DESIGN
HV CMND
24V
RTN
X8
INNER DETECTOR (8 PMT's)
THESE COMPONENTS AT ANODE POTENTIAL
PMT EMI 9825
AMPTEK 250
12 BIT 1MSPS ANALOG DEVICES AD9003
FIBER OPTIC
16 BIT SHIFT REG
XMTR
RCVR
VIRTUAL GROUND (HV)
.01/3KV
CONVERT
DIV 16
16MHZ
+15V
-15V 5V RTN
LV P/S
POWER GEN DCS8-2B
24V RTN
+HV P/S EB12 DESIGN
HV CMND
24V
RTN
FAST SIGNAL
X8
LOWER CERENKOV DETECTORS (16 PMT's)
PMT RCA 4525
AMPTEK 250
FAST SIGNAL
SIGNALS ARE COMBINED AT PMT ANODES INTO 8 PAIRS
-HV P/S EB12 DESIGN
-HV P/S EB12 DESIGN
HV CMND
24V
RTN
X8
CAMAC MODULES
CRATE CONTROLLER KENETIC SYS 3922
CAMAC / VME INTERFACE KENETIC SYS 2917
FIRST IN FIRST OUT SR KENETIC SYS 3843-J4D
12 CH 11 BIT ADC LeCROY 2249W
12 CH 11 BIT ADC LeCROY 2249W
12 CH 11 BIT ADC LeCROY 2249W
12 CH 11 BIT ADC LeCROY 2249W
DISCRIMINATOR & COINCIDENCE MODULE
FIBER OPTIC RECEIVERS (8) HFBR-2404
SHAPING & DELAY
TO TEMPERATURES VOLTAGES & PRESSURES
DRIFT SIGNALS VIA FIBER OPTIC CABLES HFBR-AWS005 (5 METERS)
VME CAGE
68030 CPU DYNATEM DC0U30-10
HOUSEKEEPING A/D DTNATEM DANA12
VME/CAMAC ADAPTOR (KS 2917)
SERIAL OUTPUT MODULE
16 MHZ CLOCK DRIVER
PARALLEL INPUT
HV CMND
FIBER OPTIC TRANSMITTERS (8) HFBR-1402
156 KBPS BI-PHASE TO TELEMETRY
COMMAND INPUTS PARALLEL
POWER BUS
24V RTN
LITHIUM BATTERY SET
TBD X 30V/30AH
DC/DC CONVERTERS
KEPCO MODELS:
24-A-5
24-A-15
24-A-15
24-A-24
SPACE SCIENCE LAB - ES62
Title
BUGS DATA SYSTEM BLOCK DIAGRAM
Size B
Document Number BUGS.BLK
REV C
Date: February 26, 1991
Sheet 1 of 1

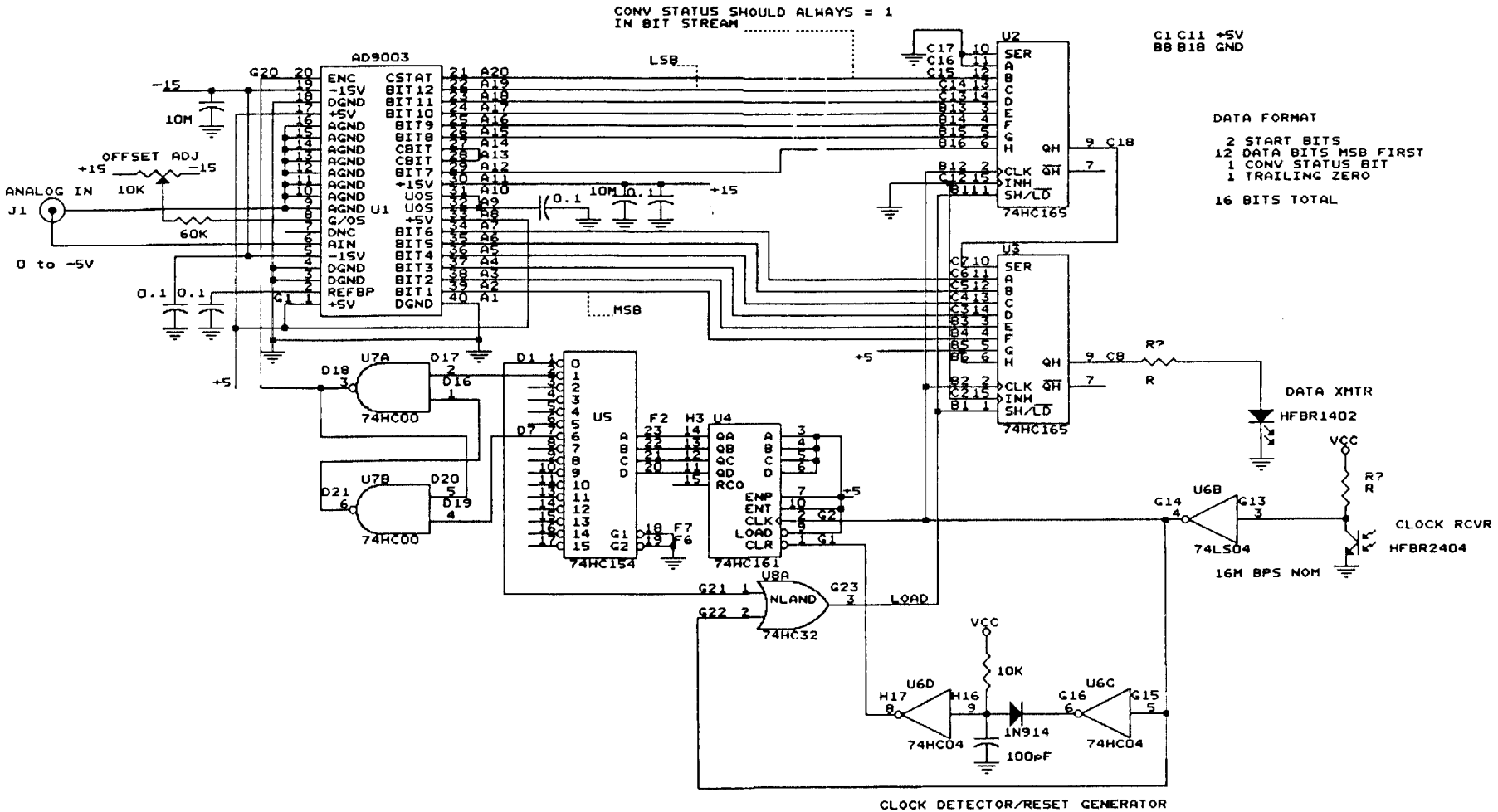

THIS ENTIRE CIRCUIT OPPERATES AT PMT ANODE POTENTIAL

SPACE SCIENCE LAB – ES62		
Title: BUGS 1 MSPS / 12 BIT ADC		
Size: B	Document Number: BUGSADC2 RWA	REV: B
Date: February 28, 1991	Sheet of	